All-Electrical Readout of Coherently Controlled Spins in Silicon Carbide

C. T.-K. Lew,[1,*] V. K. Sewani,[2] N. Iwamoto,[3] T. Ohshima,[3,4] J. C. McCallum,[1] and B. C. Johnson[5,†]
[1]School of Physics, University of Melbourne, Melbourne, Victoria 3010, Australia
[2]University of New South Wales, Kensington, New South Wales 2052, Australia
[3]National Institutes for Quantum Science and Technology, 1233 Watanuki, Takasaki 370-1292, Japan
[4]Department of Materials Science, Tohoku University, 6-6-02 Aramaki-Aza, Aoba-ku, Sendai 980-8579, Japan
[5]School of Science, RMIT University, VIC 3001, Australia

(Received 8 December 2023; accepted 20 February 2024; published 4 April 2024)

Spin defects in silicon carbide are promising candidates for quantum sensing applications as they exhibit long coherence times even at room temperature. However, spin readout methods that rely on fluorescence detection can be challenging due to poor photon collection efficiency. Here, we demonstrate coherent spin control and all-electrical readout of a small ensemble of spins in a SiC junction diode using pulsed electrically detected magnetic resonance. A lock-in detection scheme based on a three stage modulation cycle is implemented, significantly enhancing the signal-to-noise ratio. This technique enabled observation of coherent spin dynamics, specifically Rabi spin nutation, spin dephasing, and spin decoherence. The use of these protocols for magnetometry applications is evaluated.

DOI: 10.1103/PhysRevLett.132.146902

Silicon carbide (SiC) is a wide band gap semiconductor host to a broad variety of spin defects that may be employed for applications in quantum sensing and computation. Typical methods to address spin defects, such as the negatively charged silicon vacancy (V_{Si}^{-}) [1,2] and the divacancy (V_2) [3,4], employ optical excitation and fluorescence detection for spin state preparation and readout. However, this can be challenging due to the high refractive index of SiC, resulting in poor photon collection efficiency. Furthermore, many of these spin defects exhibit relatively low photoluminescence emission count rates, requiring integration into photonic structures [5,6] at the expense of additional fabrication processes.

More recently, a hybrid optical excitation and electrical readout approach has been successfully applied to V_{Si}^{-} in SiC to circumvent issues associated with optical detection [7]. This may ultimately enable better integration with supporting detection electronics, reducing size, weight, and power metrics for future devices. This electrical readout approach relies on a spin-dependent photoionization mechanism which was first applied to the nitrogen-vacancy (N-V) center in diamond [8,9].

Spin readout using electrically detected magnetic resonance (EDMR) is another well-established method for SiC defect characterization [10–16] and also for possible applications in quantum magnetometry [17,18]. However, only incoherent readout of large defect ensembles has been achieved so far. EDMR typically relies on the spin-dependent recombination (SDR) mechanism in which the device is biased into a regime where trap-assisted recombination dominates the measured current. Spin readout is then measured as a decrease in the device conductivity in resonance [19].

To further enhance magnetic-field sensing capabilities, more complex Ramsey and Hahn-echo pulse protocols might be considered for dc and ac magnetometry, respectively. In this case, the ability to coherently drive and read out the spin dynamics over time is crucial. This has not yet been achieved electrically in SiC, presumably due to the technical challenges associated with applying high power radio-frequency (rf) pulses to a fully fabricated device with metallic contacts, resulting in strong low-frequency noise and large nonresonant background current transients [20].

Here, we overcome these challenges to demonstrate all-electrical coherent spin control and readout of a small ensemble of spins in a SiC $n^{+}p$ diode using pulsed EDMR (pEDMR) at room temperature. To successfully perform coherent spin control and readout, a multistage lock-in modulation protocol is developed. We then demonstrate this protocol by performing Rabi, Ramsey, and Hahn-echo measurements, revealing an average spin dephasing time of $T_2^{\star} = 94.5 \pm 14.3$ ns, and transverse spin decoherence time of $T_2 = 1.56 \pm 0.19$ μs, respectively, at room temperature. These relatively long time constants suggest that SiC is a promising platform on which to implement dc and ac quantum sensing protocols.

A 6H-SiC n^{+}-p junction diode was used in this work. Further details on the fabrication can be found in [17]. The defects investigated in this work are formed during fabrication. Measurements were performed on a custom-built low-field pEDMR spectrometer. A simplified schematic is shown in Fig. 1(a). The multistage lock-in detection protocol employed is shown in Fig. 1(b). First, the n^{+}-p junction bias is switched between two voltages, turning the recombination current on and off. These voltages are

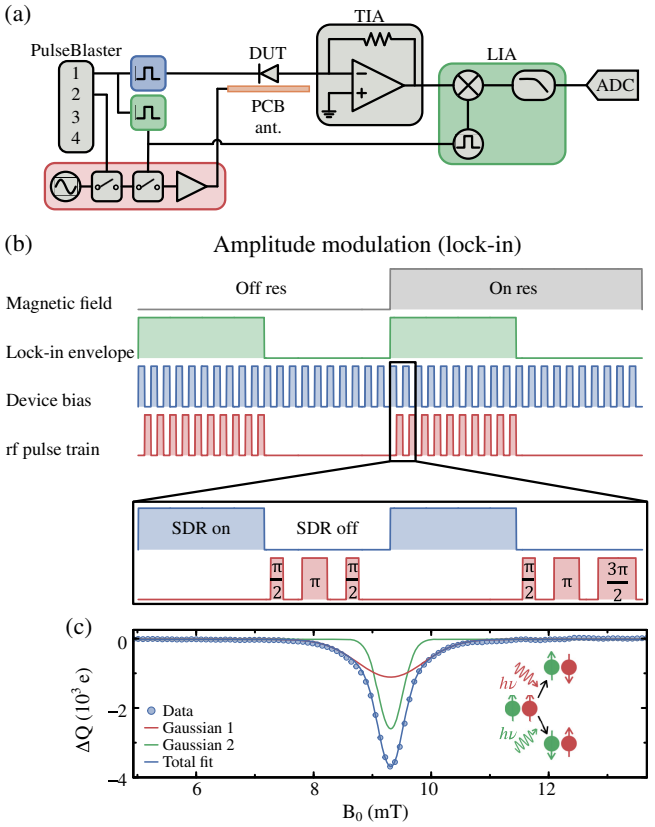

FIG. 1. (a) Schematic of the main experimental components. A description of all components is provided in the text. (b) Illustration of the amplitude modulated lock-in detection scheme for the Hahn-echo pulse sequence. (c) pEDMR spectra of the SiC diode averaged over 750 scans. A fit to the resonance signal is best described by two Gaussians corresponding to the spin manipulation of each individual spin within the spin pair, as depicted in the inset.

$V_{ON} = -2.25$ V and $V_{OFF} = -1.50$ V. During the V_{OFF} component of the sequence, a rf pulse sequence is applied to induce spin rotations after a fixed constant delay of 800 ns. The example shown in Fig. 1(b) is that of a Hahn-echo pulse sequence. Once the bias is switched back to V_{ON}, the transient current containing spin-dependent information is read out over a fixed time interval of $\Delta t = t_2 - t_1 = 10$ μs. This time interval was optimized to give the strongest spin-dependent integrated charge signal (i.e., $\Delta Q = 1/q \int_{t_1}^{t_2} \Delta I dt$). The sequence is repeated over N repetitions and encoded inside a low-frequency lock-in amplifier (LIA) envelope at $f_{\mathrm{mod}} = 178.57$ Hz, within the bandwidth of the transimpedance amplifier (TIA). This amplitude modulates the rf pulse train. Synchronicity across all test instruments is maintained using a PulseBlaster programmable TTL pulse generator.

For pulse sequences employing multiple rf pulses, such as the Hahn-echo pulse sequence depicted in Fig. 1(b), the final $\pi/2$ spin projection pulse is alternated between $\pi/2$ and $3\pi/2$ pulses. To remove the effects of varying overall rf pulse widths, the entire sequence is repeated off resonance by alternating the background magnetic field [7]. The final spin signal is obtained by subtracting the on-resonance ($B_{\mathrm{res}} = 9.31$ mT) from the off-resonance ($B_{\mathrm{off}} = 3.22$ mT) signal and subtracting the $3\pi/2$ signal from the $\pi/2$ signal.

Figure 1(c) shows the pEDMR spectrum of the SiC n^+-p junction diode. The spectrum was constructed after averaging over 750 magnetic field sweeps using a rf pulse duration, frequency, and power of $\tau_p = 60$ ns, $f = 263$ MHz and $P_{\mathrm{rf}} = 25$ W, respectively. The peak amplitude corresponds to approximately $\Delta Q = 3615$ charges, while the noise floor for this particular measurement corresponds to a detectability limit of approximately 13 spins.

The resonance peak can be fitted with two Gaussians. In the SDR mechanism prior to electron-hole pair recombination, an intermediate electrostatically bound spin pair forms between a conduction band electron and a spin defect, which exists in one of four energy eigenstates [19]. Following a resonant rf pulse, either spin in the spin pair coherently precesses in the B_1 excitation field, altering the permutation symmetry of the spin pair [inset of Fig. 1(c)]. This is electrically read out as a change in the device conductivity, which is proportional to a change in the recombination rates [21]. These individual spins experience a slightly different hyperfine interaction with the surrounding nuclear spin bath from its spin partner, resulting in different linewidths [22].

Coherent control of the spin pairs can now be achieved by performing Rabi oscillation measurements and monitoring the integrated charge as a function of increasing resonant rf pulse duration τ_p [Fig. 2(a)]. A complex oscillatory behavior is observed and is well described by [23],

$$\Delta Q(\tau_p) = [\Delta Q_1 T(\kappa_1 \gamma B_1 \tau_p) + \Delta Q_2 T(\kappa_2 \gamma B_1 \tau_p)] e^{-\tau_p / T^{\star}_{2,\mathrm{Rabi}}}, \quad (1)$$

where $T(\alpha)$ is the transient function given by $T(\alpha) = \pi \int_0^{\alpha} J_0(2x)\, dx$, with J_0 the Bessel function of the first kind [21,24]. The turning angle $\alpha = \kappa \gamma B_1 \tau_p$ is dependent on the Rabi frequency $\Omega = \gamma B_1$. The ratio κ_2/κ_1 is related to the spin multiplicity and has a value of 2 according to the fit, suggesting that the spin pair is weakly coupled.

As illustrated in the inset of Fig. 2(a), the transient function oscillating at Ω describes the case where only one electron spin in the spin pair is excited. On the other hand, the transient function oscillating at 2Ω describes both spins oscillating simultaneously when the applied B_1 field strength is greater than the Larmor separation between the two spins, leading to a beating oscillation.

The complex oscillatory behavior is sustained over four cycles in Fig. 2(a) and is heavily dampened by an exponential decay characterized by a spin dephasing time, $T^{\star}_{2,\mathrm{Rabi}} = 263 \pm 13$ ns, determined from the fit to the

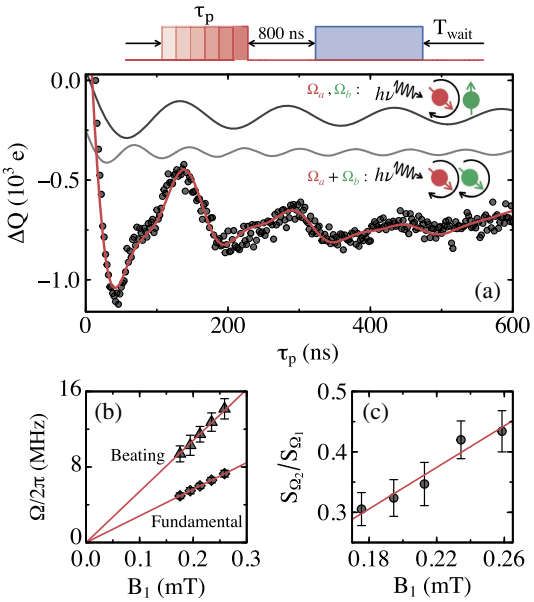

FIG. 2. (a) Electrically detected Rabi oscillations for $P_{\mathrm{rf}} = 50$ W. The pulse sequence is shown above (a). A fit to the data using Eq. (1) (red curve) highlights spin beating at the fundamental and harmonic frequencies. The deconvoluted frequencies are plotted separately with a y-axis offset for clarity and its corresponding spin-pair mechanism is depicted. (b) The fundamental and beating frequency as a function of B_1. (c) Ratio between $S_{\Omega 2}$ and $S_{\Omega 1}$ as a function of B_1. A linear dependence and the low ratio below unity suggests a weakly exchanged coupled spin pair.

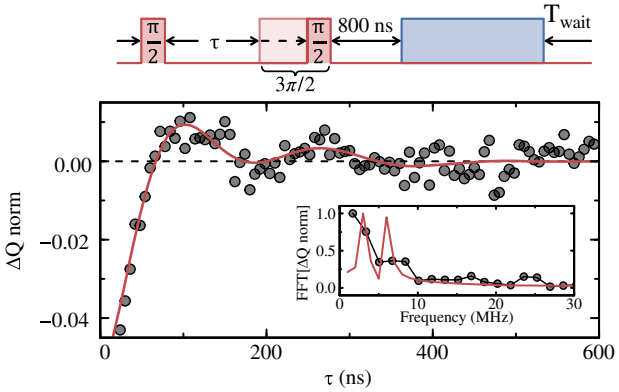

FIG. 3. Normalized integrated charge in response to the Ramsey pulse sequence indicated above the main figure measured as a function of τ at 0.08 mT off resonance. The solid red line is a fit to the data following Eq. (2) and the fast Fourier transform (FFT) frequency spectrum is shown in the inset.

experimental data using Eq. (1). This defines the duration over which the singlet-triplet spin transitions in the spin-pair ensemble can be driven before it dephases into mixed states due to the B_1 field inhomogeneity over the device under test (DUT).

A series of Rabi oscillation measurements were performed under various rf powers and the frequency components were determined from fits using Eq. (1), as shown in Fig. 2(b). Estimates of the B_1 driving field strength for each rf power considered were obtained from the Rabi frequencies of the fundamental component corresponding to the spin nutation of a single $S = 1/2$ spin, following the expected $\sqrt{P_{\mathrm{rf}}} \propto B_1$ dependence. Both the fundamental and harmonic frequency components increase linearly as a function of the B_1 driving field strength, with the slope of the beating component twice the slope of the fundamental component.

The presence of a 2Ω component can arise either from nonselective excitation of a weakly coupled spin pair in which the amplitude of the spin-beating component is dependent on the B_1 driving field strength, or for a purely strongly exchanged coupled spin pair with the 2Ω component independent of the B_1 driving field strength [25]. To determine which, we plot the ratio between the amplitude of the 2Ω and Ω component, $S_{\Omega 2}/S_{\Omega 1}$, as a function of B_1 in Fig. 2(c). The consistently low amplitude ratio below unity and the linear dependence on B_1 suggest that the 2Ω component is a result of weakly coupled spin-pair spin beating [26].

To further demonstrate the applicability of the lock-in detection scheme, we apply the Ramsey pulse protocol and characterize the spin dynamics of the ensemble spin-pair system. Figure 3 shows an example Ramsey fringe measured slightly detuned off resonance at $B_{\mathrm{res}} - B_0 = 0.080 \pm 0.008$ mT ($\sim 2.25 \pm 0.23$ MHz) by varying the free precession time τ. The pulse sequence is indicated above Fig. 3. A $\pi/2$ pulse length of 34 ns was determined from Fig. 2. Here, the normalized signal is based on the measured raw integrated charge using the $\pi/2$ and $3\pi/2$ pulse [i.e., ΔQ norm $= (\Delta Q_{\pi/2} - \Delta Q_{3\pi/2})/(\Delta Q_{\pi/2} + \Delta Q_{3\pi/2})$].

An oscillation in the integrated charge superimposed with a strong exponential decay envelope is observed and can be described by [9,27],

$$\Delta Q(\tau) = A e^{(-\tau/T^{\star}_{2,\mathrm{FID}})^n} \sum_{i=1}^{N} \cos(2\pi\delta_i \tau + \phi_i), \qquad (2)$$

where n is a stretched exponential parameter, δ_i are the detuning oscillation frequencies, ϕ_i are the phase shifts, and A is a fitting parameter. The stretched exponential parameter takes on a value between 1 and 2, with the limits corresponding to a purely Lorentzian and Gaussian resonance line shape, respectively. A fit using Eq. (2) (red curve in Fig. 3) gives $n = 2$ (Gaussian), and $T^{\star}_{2,\mathrm{FID}} = 94.5 \pm 14.3$ ns. The Fourier transform of the data and the fit are provided in the inset of Fig. 3, showing two Fourier components at $\delta_1 = 2.27 \pm 0.16$ MHz and $\delta_2 = 5.26 \pm 0.18$ MHz. These correspond to 0.081 ± 0.006 mT and 0.187 ± 0.006 mT in units of magnetic field detuned from resonance. The first oscillation frequency is consistent with the slight detuning off resonance used to perform the

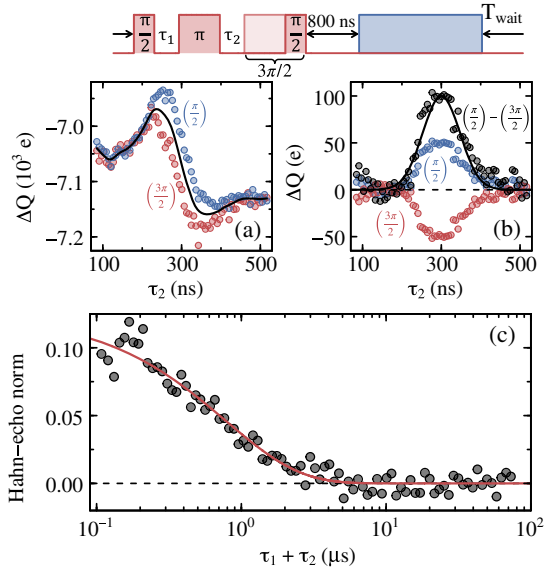

FIG. 4. (a) Raw integrated charge in response to the Hahn-echo pulse sequence as a function of τ_2, with $\tau_1 = 300$ ns for the $\pi/2$ (blue symbols) and $3\pi/2$ (red symbols) spin projection pulse. The background offset is also included (black curve). (b) Subtraction of the raw integrated charge between the two traces obtained from the $\pi/2$ and $3\pi/2$ spin projection pulse, revealing a Hahn-echo response (black symbols) following a Gaussian distribution (black curve). The individual Hahn-echo responses from the $\pi/2$ and $3\pi/2$ spin projection pulse after background subtraction [black curve in (a)] are also shown for comparison. (c) Spin decoherence measurement, with the normalized integrated charge measured as a function of $\tau_1 + \tau_2$. The solid red line is a fit to the data using Eq. (3).

Ramsey measurement, whereas the second oscillation frequency describes the detuning off resonance for the second electron in the spin pair, consistent with the description of a weakly coupled spin pair excited nonselectively and simultaneously.

Last, the spin decoherence of the spin-pair ensemble probed is characterized by applying the Hahn-echo pulse sequence. Figure 4(a) shows the individual raw integrated charge utilizing a $\pi/2$ (blue symbols) and $3\pi/2$ (red symbols) spin projection pulse for phase cycling as a function of τ_2 with $\tau_1 = 300$ ns. The pulse sequence is drawn above this plot. A large background offset (black curve) determined by the average of the two traces is observed, covering the Hahn-echo signal of interest. The Hahn-echo signal is recovered when the two traces are subtracted from one another, as shown in Fig. 4(b) (black symbols), revealing a negative echo amplitude. For completeness, the individual Hahn-echo traces after background offset subtraction are also shown.

By fixing $\tau_1 = \tau_2$ and varying the total evolution time $\tau_1 + \tau_2$, spin decoherence can be characterized. Figure 4(c) shows the normalized Hahn-echo amplitude as a function of $\tau_1 + \tau_2$. A decay in the normalized Hahn-echo amplitude is observed following a stretched exponential of the form,

$$\Delta Q(\tau) = A \exp(-2\tau/T_2)^n, \tag{3}$$

with $T_2 = 1.56 \pm 0.19$ μs and $n = 0.85 \pm 0.11$ determined from the fit. The stretched exponential parameter in a Hahn-echo measurement describes the homogeneity of the ensemble spin pair measured, with each spin pair in the ensemble having its own spin-spin coupling strength and recombination rate. A value of $n = 0.85 \pm 0.11$ suggests a relatively uniform spin-pair ensemble distribution.

The protocols developed here lend themselves to applications in quantum magnetometry. The magnetic field sensitivity using Ramsey and Hahn-echo pulse protocols is governed by the spin dephasing (Fig. 3) and spin decoherence (Fig. 4), respectively. The shot-noise-limited sensitivity based on the Ramsey and Hahn-echo protocols is described for optical-based measurements in Ref. [28]. This can be generalized to electrical readout by considering the electrical shot noise instead. Generally, the optimal Ramsey dc sensitivity is achieved when $\tau \sim T_2^\star$ up to a signal frequency of $\nu \sim 1/T_2^\star$. Similarly, the optimal Hahn-echo ac sensitivity is achieved when $\tau \sim T_2$ exclusively for magnetic fields oscillating at $\nu \sim 1/T_2$. Longer T_2 times and thus smaller minimum detectable ac magnetic field may be achieved by implementing the Carr-Purcell-Meiboom-Gill [29] pulse sequence at the expense of a reduced bandwidth. The final key factor to achieve practical magnetometry is the acquisition time of the measurement. At present, signal averaging is essential and this currently inhibits real-time magnetometry. However, further signal optimization could be accomplished through photocurrent and common mode rejection techniques [17] or via an increase in the defect density. Optimization of the device geometry may also aid in more efficient spin readout.

In summary, we have experimentally demonstrated all-electrical coherent spin control and readout of an ensemble of spins in a SiC p-n junction diode using a multistage lock-in detection scheme for pEDMR. Using the lock-in detection scheme, the spin properties of the ensemble spin pair were characterized. Analysis of the Rabi oscillations revealed the individual electron spins in the spin pair within the ensemble are weakly coupled to each other, but are nonselectively driven simultaneously, resulting in the spin beating at twice the Rabi oscillation frequency. The Ramsey pulse sequence was then applied to characterize the spin dephasing time, which was found to be equal to $T_2^\star = 94.5 \pm 14.3$ ns. Last, the spin decoherence time was determined to be $T_2 = 1.56 \pm 0.19$ μs utilizing the Hahn-echo pulse sequence. These results are discussed in the context of magnetometry.

It is expected the lock-in detection scheme demonstrated here is transferable to studying other spin defect and material systems. Furthermore, the scheme is compatible with other more advanced pulse sequences that, for example, explore nuclear spin interactions, such as

electron-nuclear double resonance [30], motivating a range of future studies.

The authors thank D. L. Creedon, S. Gregory, and S. A. Yanni for their technical support during the development and construction of the low-field EDMR spectrometer. C. T.-K. Lew acknowledges the Australian Government Research Training Program Scholarship. T. O. acknowledges JSPS KAKENHI No. 21H04553 and No. 20H00355.

*Corresponding author: christopher.lew@unimelb.edu.au
†brett.johnson2@rmit.edu.au

[1] V. A. Soltamov, A. A. Soltamova, P. G. Baranov, and I. I. Proskuryakov, Room temperature coherent spin alignment of silicon vacancies in 4*H*- and 6*H*-SiC, Phys. Rev. Lett. **108**, 226402 (2012).
[2] M. Niethammer, M. Widmann, S.-Y. Lee, P. Stenberg, O. Kordina, T. Ohshima, N. T. Son, E. Janzén, and J. Wrachtrup, Vector magnetometry using silicon vacancies in 4*H*-SiC under ambient conditions, Phys. Rev. Appl. **6**, 034001 (2016).
[3] W. F. Koehl, B. B. Buckley, F. J. Heremans, G. Calusine, and D. D. Awschalom, Room temperature coherent control of defect spin qubits in silicon carbide, Nature (London) **479**, 84 (2011).
[4] H. Seo, A. L. Falk, P. V. Klimov, K. C. Miao, G. Galli, and D. D. Awschalom, Quantum decoherence dynamics of divacancy spins in silicon carbide, Nat. Commun. **7**, 12935 (2016).
[5] M. Widmann, S.-Y. Lee, T. Rendler, N. T. Son, H. Fedder, S. Paik, L.-P. Yang, N. Zhao, S. Yang, I. Booker *et al.*, Coherent control of single spins in silicon carbide at room temperature, Nat. Mater. **14**, 164 (2015).
[6] A. L. Crook, C. P. Anderson, K. C. Miao, A. Bourassa, H. Lee, S. L. Bayliss, D. O. Bracher, X. Zhang, H. Abe, T. Ohshima *et al.*, Purcell enhancement of a single silicon carbide color center with coherent spin control, Nano Lett. **20**, 3427 (2020).
[7] M. Niethammer, M. Widmann, T. Rendler, N. Morioka, Y.-C. Chen, R. Stöhr, J. U. Hassan, S. Onoda, T. Ohshima, S.-Y. Lee, A. Mukherjee, J. Isoya, N. T. Son, and J. Wrachtrup, Coherent electrical readout of defect spins in silicon carbide by photo-ionization at ambient conditions, Nat. Commun. **10**, 5569 (2019).
[8] E. Bourgeois, A. Jarmola, P. Siyushev, M. Gulka, J. Hruby, F. Jelezko, D. Budker, and M. Nesladek, Photoelectric detection of electron spin resonance of nitrogen-vacancy centres in diamond, Nat. Commun. **6**, 8577 (2015).
[9] M. Gulka, E. Bourgeois, J. Hruby, P. Siyushev, G. Wachter, F. Aumayr, P. R. Hemmer, A. Gali, F. Jelezko, M. Trupke *et al.*, Pulsed photoelectric coherent manipulation and detection of N-*V* center spins in diamond, Phys. Rev. Appl. **7**, 044032 (2017).
[10] C. T.-K. Lew, V. K. Sewani, T. Ohshima, J. C. McCallum, and B. C. Johnson, Charge pumping electrically detected magnetic resonance of silicon carbide power transistors, J. Appl. Phys. **134**, 055703 (2023).
[11] T. Umeda, T. Kobayashi, M. Sometani, H. Yano, Y. Matsushita, and S. Harada, Carbon dangling-bond center (carbon P_b center) at 4*H*-SiC $(0001)/SiO_2$ interface, Appl. Phys. Lett. **116**, 071604 (2020).
[12] T. Umeda, Y. Kagoyama, K. Tomita, Y. Abe, M. Sometani, M. Okamoto, S. Harada, and T. Hatakeyama, Electrically detected-magnetic-resonance identifications of defects at 4*H*-SiC $(0001^-)/SiO_2$ interfaces with wet oxidation, Appl. Phys. Lett. **115**, 151602 (2019).
[13] G. Gruber, J. Cottom, R. Meszaros, M. Koch, G. Pobegen, T. Aichinger, D. Peters, and P. Hadley, Electrically detected magnetic resonance of carbon dangling bonds at the Si-face 4*H*-SiC/SiO_2 interface, J. Appl. Phys. **123**, 161514 (2018).
[14] J. Cottom, G. Gruber, G. Pobegen, T. Aichinger, and A. Shluger, Recombination defects at the 4*H*-SiC/SiO_2 interface investigated with electrically detected magnetic resonance and *ab initio* calculations, J. Appl. Phys. **124**, 045302 (2018).
[15] C. J. Cochrane, P. M. Lenahan, and A. J. Lelis, Identification of a silicon vacancy as an important defect in 4H SiC metal oxide semiconducting field effect transistor using spin dependent recombination, Appl. Phys. Lett. **100**, 023509 (2012).
[16] M. Anders, P. Lenahan, and A. Lelis, Are dangling bond centers important interface traps in 4*H*-SiC metal oxide semiconductor field effect transistors?, Appl. Phys. Lett. **109**, 142106 (2016).
[17] C.-K. Lew, V. Sewani, N. Iwamoto, T. Ohshima, J. McCallum, and B. Johnson, Enhanced magnetometry with an electrically detected spin defect ensemble in silicon carbide, Appl. Phys. Lett. **122**, 234001 (2023).
[18] C. J. Cochrane, J. Blacksberg, M. A. Anders, and P. M. Lenahan, Vectorized magnetometer for space applications using electrical readout of atomic scale defects in silicon carbide, Sci. Rep. **6**, 37077 (2016).
[19] D. Kaplan, I. Solomon, and N. Mott, Explanation of the large spin-dependent recombination effect in semiconductors, J. Phys. Lett. **39**, 51 (1978).
[20] F. Hoehne, L. Dreher, J. Behrends, M. Fehr, H. Huebl, K. Lips, A. Schnegg, M. Suckert, M. Stutzmann, and M. S. Brandt, Lock-in detection for pulsed electrically detected magnetic resonance, Rev. Sci. Instrum. **83**, 043907 (2012).
[21] C. Boehme and K. Lips, Theory of time-domain measurement of spin-dependent recombination with pulsed electrically detected magnetic resonance, Phys. Rev. B **68**, 245105 (2003).
[22] D. R. McCamey, K. J. van Schooten, W. J. Baker, S.-Y. Lee, S.-Y. Paik, J. M. Lupton, and C. Boehme, Hyperfine-field-mediated spin beating in electrostatically bound charge carrier pairs, Phys. Rev. Lett. **104**, 017601 (2010).
[23] X. Liu, H. Popli, O. Kwon, H. Malissa, X. Pan, B. Park, B. Choi, S. Kim, E. Ehrenfreund, C. Boehme, and Z. V. Vardeny, Isotope effect in the magneto-optoelectronic response of organic light-emitting diodes based on donor–acceptor exciplexes, Adv. Mater. **32**, 2004421 (2020).
[24] S.-Y. Paik, S.-Y. Lee, W. J. Baker, D. R. McCamey, and C. Boehme, T_1 and T_2 spin relaxation time limitations of phosphorous donor electrons near crystalline silicon to silicon dioxide interface defects, Phys. Rev. B **81**, 075214 (2010).

[25] H. Morishita, W. J. Baker, D. P. Waters, R. Baarda, J. M. Lupton, and C. Boehme, Mechanisms of spin-dependent dark conductivity in films of a soluble fullerene derivative under bipolar injection, Phys. Rev. B **89**, 125311 (2014).

[26] A. Gliesche, C. Michel, V. Rajevac, K. Lips, S. D. Baranovskii, F. Gebhard, and C. Boehme, Effect of exchange coupling on coherently controlled spin-dependent transition rates, Phys. Rev. B **77**, 245206 (2008).

[27] J. Lu, F. Hoehne, A. R. Stegner, L. Dreher, M. Stutzmann, M. S. Brandt, and H. Huebl, High-resolution electrical detection of free induction decay and Hahn echoes in phosphorus-doped silicon, Phys. Rev. B **83**, 235201 (2011).

[28] J. F. Barry, J. M. Schloss, E. Bauch, M. J. Turner, C. A. Hart, L. M. Pham, and R. L. Walsworth, Sensitivity optimization for N-*V*-diamond magnetometry, Rev. Mod. Phys. **92**, 015004 (2020).

[29] S. Meiboom and D. Gill, Modified spin-echo method for measuring nuclear relaxation times, Rev. Sci. Instrum. **29**, 688 (1958).

[30] T. Nishikawa, N. Morioka, H. Abe, H. Morishita, T. Ohshima, and N. Mizuochi, Electrical detection of nuclear spins via silicon vacancies in silicon carbide at room temperature, Appl. Phys. Lett. **121**, 184005 (2022).